Pinning mass-selected Ag_n clusters on the $TiO_2(110)-1\times1$ surface via deposition at high kinetic energy

Xiao Tong, Lauren Benz, Steeve Chrétien, Paul Kemper, Andrei Kolmakov, Horia Metiu, Michael T. Bowers, and Steven K. Buratto[a)]
Department of Chemistry and Biochemistry, University of California, Santa Barbara, California 93106

(Received 25 July 2005; accepted 20 September 2005; published online 18 November 2005)

We present the first scanning tunneling microscopy (STM) study of the deposition of mass-selected silver clusters ($Ag_n, n=1, 2, 3$) on a rutile $TiO_2(110)-1\times1$ surface at room temperature under hard-landing conditions. Under hard-landing conditions, only small features are observed on the surface in all cases without sintering or surface damage. This suggests that the high impact energy of the clusters mainly dissipates as thermal energy in the substrate, resulting in the recovery of any initial impact-induced surface damage and the formation of bound clusters on the surface near the impact point. STM images indicate that Ag_1 binds on the bridging oxygen rows twice as often as on the Ti rows. Density-functional Theory (DFT) calculations are consistent with Ag_1 binding at either bridging oxygen vacancies or with two adjacent bridging oxygen atoms in the same bridging oxygen row. STM images of Ag_2 and Ag_3 depositions indicate almost exclusive binding centered on the Ti-atom rows. DFT calculations suggest that the Ag_2 and Ag_3 clusters are bound between two bridging oxygen rows, which is consistent with the STM observations. © *2005 American Institute of Physics*. [DOI: 10.1063/1.2118587]

I. INTRODUCTION

Nanoparticle size is a critical parameter in the catalytic behavior of metal/oxide catalysts.[1–4] The size distribution of the clusters formed in conventional vapor deposition experiments is not well defined due to the inherent size distribution coming from the cluster source, and cluster diffusion and aggregation which occurs after landing on the substrate.[5] For the purpose of studying the size dependence of catalytic activity, not only is size selection a prerequisite in cluster deposition experiments, but the preservation of the incoming cluster upon deposition is also important.[6,7] Low-energy cluster deposition (a few eV/atom) on metal surfaces often leads to cluster diffusion and aggregation resulting in the formation of large clusters and islands; thus the cluster size in the gas phase is not preserved.[8] High-energy cluster deposition (~100 eV/atom) can prevent diffusion and aggregation of the incoming clusters, however, the energy which is released during the impact can be sufficient to fragment the cluster, to create substrate damage, or to embed the cluster in the bulk.[9–12]

In this work, we report the deposition of size-selected Ag_1, Ag_2, and Ag_3 clusters on a $TiO_2(110)$-(1×1) surface at high impact energies. To do this, we have utilized atomic resolution scanning tunneling microscopy (STM) to observe the surface morphology after cluster deposition, and have employed density-functional theory (DFT) calculations to explore the possible cluster adsorption geometries. This work suggests a new mechanism for pinning mass-selected clusters on the surface.

[a)]Author to whom correspondence should be addressed. Fax: 1-805-893-4120. Electronic mail: buratto@chem.ucsb.edu

II. EXPERIMENT

All experiments were performed in an ultrahigh vacuum (UHV) chamber equipped with an RHK-100 variable-temperature STM with a base pressure of less than 2×10^{-10} torr, and a cluster deposition chamber with maximum deposition pressure $<1\times10^{-9}$ torr. The clean $TiO_2(110)$-(1×1) surface was prepared by multiple cycles of Ar^+-ion sputtering (1 keV, 20 min), followed by annealing at 900 K for 20 min. This procedure produced a surface with an average terrace of width of 25 nm.

The production of size-selected clusters is described in detail elsewhere.[13] Briefly, a pulsed, frequency-doubled yttrium aluminum garnet (YAG) laser beam (532 nm, 500 mJ/pulse max power) is focused on a rotating, translating silver rod, producing a silver plasma. Following the laser pulse, a pulse of argon enters the source cavity, inducing $Ag_n^+ \times(n=1,2,3\ldots)$ cluster formation. The clusters are then accelerated from the source through several focusing and steering lenses into a magnetic-field analyzer where the size-selection process occurs. The mass-selected cluster beam is then guided onto the sample of titania in the cluster deposition chamber. In the work reported here, the incident energy for the monomer, dimer, and trimer are controlled to be +175 eV $\times$(±1.5, ±3.5, and ±6 eV, respectively). A typical beam intensity is 1.0 nA/cm^2, leading to exposure times of 20–60 min (depending on cluster size) for ~1.5% coverage [relative to Au(111) surface]. The deposited sample is then transferred into an STM chamber for inspection. STM images are obtained in constant current mode, at sample biases between +1 and +2 V, and tunneling currents between 0.1 and 0.2 nA. The electrons tunnel from the tip into the

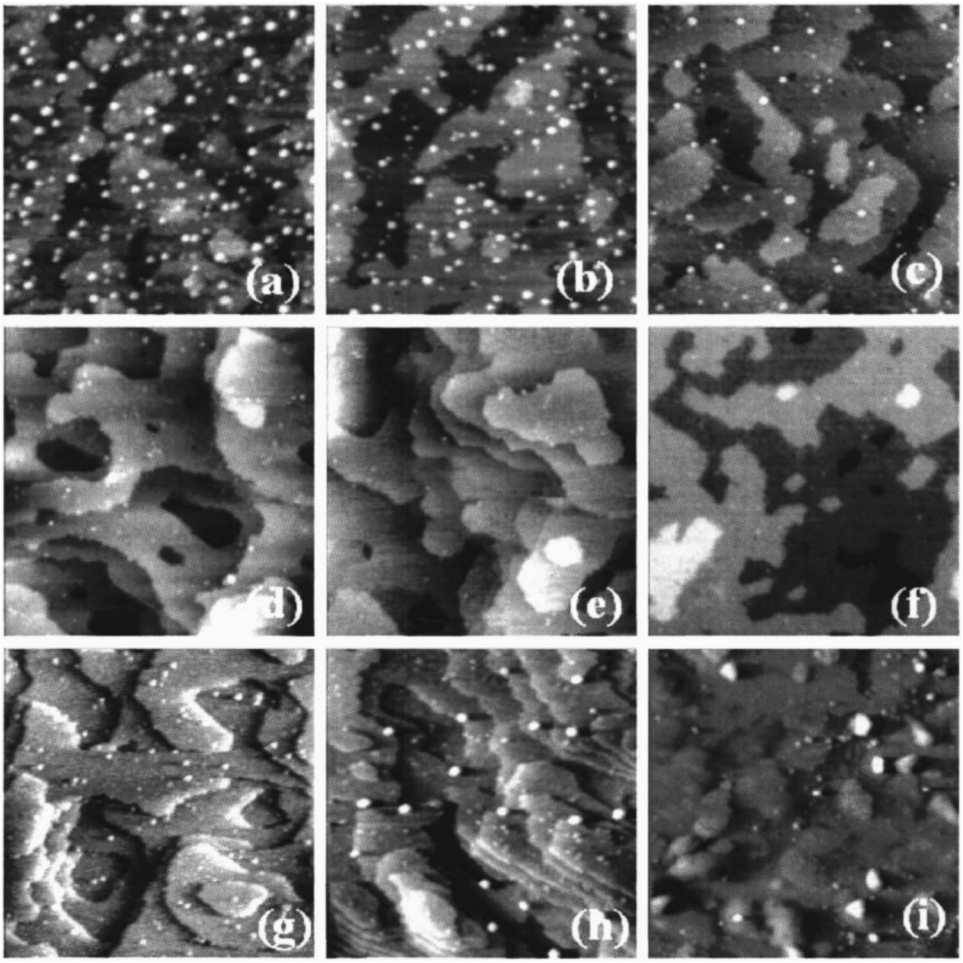

FIG. 1. STM images [(a)–(c)] show a clean $TiO_2(110)-1\times1$ surface after exposing to Ag_1, Ag_2, and Ag_3, respectively, under soft-landing conditions. Images [(d)–(f)] show the same atomic exposure of Ag_1, Ag_2, and Ag_3 under hard-landing conditions (respectively). Large clusters are rarely observed in the case of hard landing in contrast to the soft-landing experiments. Images [(g)–(i)] show large clusters appearing on the respective hard-landed surface upon annealing to about 600 K for 15–30 s. The scale of all images is 100×100 nm^2.

empty states of the surface. The STM tips are made from electrochemically etched tungsten wire and are subsequently cleaned in UHV by electron bombardment.

III. COMPUTATIONAL DETAILS

We have performed periodic Kohn-Sham density-functional theory calculations using the generalized gradient approximation[14,15] and the VASP program.[16–19] The ionic cores were described by scalar relativistic ultrasoft pseudopotentials.[20] The cutoff in the plane-wave expansion was 270 eV. Tests were performed with a larger cutoff (396 eV) to ensure that the results are converged with the lower cutoff. We sampled the Brillouin zone at the Γ point only. We have taken into account the monopole, dipole, and quadrupole corrections to the energy using a modified version of the method proposed by Makov and Payne.[21] We allowed fractional occupancies of the bands by using a window of 0.05 eV. The $TiO_2(110)$ surface was modeled by a $[3\times2]$ supercell. We removed one of the six protruding bridging oxygen atoms to represent the defective (reduced) surface. This corresponds to a concentration of 17% oxygen atom vacancies, which is slightly larger than the experimental value ($\sim10\%$). Many starting structures were initially optimized on a slab composed of six layers (two triple layers). All the lowest-energy structures located in a window of 1 eV were optimized again on a 12-layer (four triple-layers) slab. The adsorption of Ag clusters takes place on only one side of the $TiO_2(110)$ slab in a vacuum space of 17 Å. All the structures were completely relaxed except the bottom triple layer of $TiO_2(110)$ which was fixed to the bulk position. The convergence criterion was 10^{-4} eV for the self-consistent electronic minimization and for the change of the total free energy between two consecutive ionic steps. The transition states were located using the nudged elastic band.[22]

We use the term desorption energy (D_e), as is common in surface science, to describe the binding strength between Ag clusters and the rutile $TiO_2(110)$ surface. For example, the desorption energy of Ag_2 adsorbed on a stoichiometric surface is

$$D_e[\mathrm{Ag_2}] = E[\mathrm{TiO_2(perfect)}] + E[\mathrm{Ag_2}] - E[\mathrm{Ag_2/TiO_2(perfect)}].$$

$E[\mathrm{TiO_2(perfect)}]$ and $E[\mathrm{Ag_2/TiO_2(perfect)}]$ are the total energies of the stoichiometric $TiO_2(110)$ surface without and with Ag cluster adsorbed on it, while $E[\mathrm{Ag_2}]$ is the total energy of Ag_2 in the gas phase.

IV. EXPERIMENTAL RESULTS

As shown in Figs. 1(a)–1(c), STM images reveal large clusters after the depositions of Ag_1, Ag_2, and Ag_3 with impact energies of a few eV (soft-landing conditions), indicating the adsorption, diffusion, and aggregation of clusters under these circumstances. For the trimer there is also a high

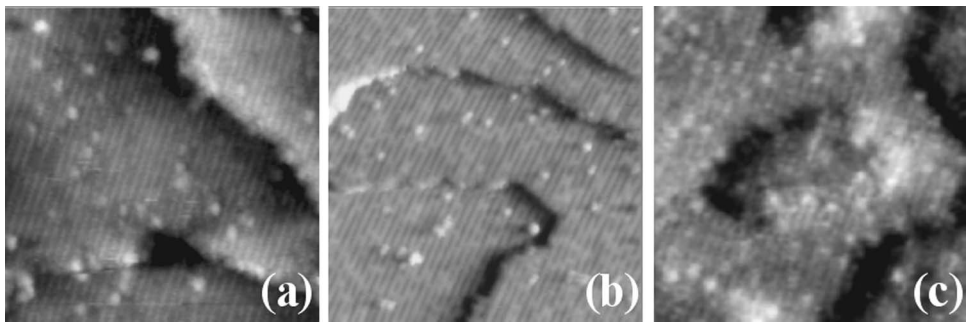

FIG. 2. STM images show the presence of small clusterlike features appearing in (a), (b), and (c) as bright protrusions upon the hard landing of Ag_1, Ag_2, and Ag_3, respectively. The scale of all images is 50×50 nm^2.

density of small clusters present on the surface (attributed to intact trimers), while the monomer and dimer depositions do not show this feature.[23] Figures 1(d)–1(f) show STM images of the surface morphology following the deposition of Ag_1, Ag_2, and Ag_3 with incident energies near 175 eV (hard-landing conditions). Large sintered clusters are rarely observed. After annealing to ~600 K for 15–30 s, large clusters appear on the surface due to sintering as shown in Figs. 1(g)–1(i). This indicates that the adsorbed metal is mobile on the surface at high temperatures, which is consistent with soft-landing and vapor-deposited clusters. It is important to note that we see no additional metal appears on the surface upon annealing, suggesting that there are no embedded clusters in our experiments.

High-resolution STM images in Figs. 2(a)–2(c) and Figs. 3(a)–3(c) show the presence of bright protrusions, which are attributed to small Ag clusters on the surface after exposure to Ag_1^+, Ag_2^+, and Ag_3^+, respectively. The bright rows of the substrate are the fivefold-coordinated Ti atoms (5*c*-Ti) and the dark rows are the bridging oxygen atoms.[24] A number of important observations can be made from the images in Figs. 2 and 3. Under hard-landing conditions [Figs. 2(a) and 3(a)] we observe two binding sites for the Ag_1 atoms. The first site is on the bridging oxygen rows [black arrow in Fig. 3(a)]. The second site is on the 5*c*-Ti rows (white arrow). Analyzing many such images we found that 65% of the Ag atoms are found on the bridging oxygen rows and 35% are found on the 5*c*-Ti rows. These statistics are summarized in Table I and compared to the depositions of Ag_2 and Ag_3.

In sharp contrast to the monomer, the deposition of Ag_2 clusters under hard-landing conditions [Figs. 2(b) and 3(b)] results in a distribution of 89% on the 5*c*-Ti rows and 11% on bridging oxygen rows. For Ag_3 [Figs. 2(c) and 3(c)] we observe 96% centered on the 5*c*-Ti rows. Slight differences in the measured heights on the 5*c*-Ti rows in the case of the Ag_2 and Ag_3 depositions (1.36 Å vs 1.03 Å) imply a possible difference in their electronic structure and/or adsorption geometries.

It is important to note that all of the bright protrusions centered on the bridging oxygen rows appear to be greater in height than oxygen vacancies (~1.75 Å vs ~0.4 Å, respectively), and all of the bright features on the Ti rows are greater in height than intrinsic type *B*(~−0.4 Å) and *C* defects (~0.6 Å),[24,25] indicating that they are not deposition-induced defects. In fact, there is neither an increase of intrinsic defects nor any observable surface damage in the STM images after hard landing the clusters. Among the intrinsic defects the bridging oxygen vacancies are easiest to produce, and a high density of oxygen vacancy defects can result in the formation of 1×2 strands on the surface, or even entire surface reconstruction to the 1×2 phase.[26] After thermally desorbing all of the hard-landed clusters from surface, we observe no increased density of oxygen vacancies or 1×2 reconstructions compared to the surface prior to deposition.

V. DISCUSSION

Langevin molecular-dynamics (MD) simulations of Mo_{1000} clusters impinging on a Mo substrate with a total collision energy of ~5–10 keV,[27,28] indicate that a small high-temperature spot is formed at each impact location for a very short time. All of the initial impact-induced defects around the impact zone are annealed during cooling, resulting in near epitaxial growth of clusters on the substrate. A similar mechanism has been found in MD simulations of the impact of energetic Al clusters on a Cu(111) surface.[29] Elastic surface recovery without a phase change around the impact zone has also been found in MD simulations of clusters containing 960 CO_2 molecules impinging on a diamond surface with a total impact energy of 10 keV.[30]

Based on our STM images and the above mentioned MD simulations, we conclude that the high impact energy of clusters is mainly dissipated as thermal energy to the substrate and to the cluster itself, resulting in the recovery of the initial desorption-induced surface damage around the impact point. Initially an incident monomer may be implanted a few layers beneath the surface, resulting in a distortion of surface structure. However, during cooling the distorted surface recovers to a normal 1×1 surface and the embedded silver atom emerges from the bulk, eventually residing on the surface. The cluster beam intensity in our experiments is ~1.0 nA/cm^2, therefore a cluster strikes a 1 Å^2 spot on the surface every 1.5×10^6 s. Consequently, the surface is able to relax before the next collision due to the low flux. If this relaxation process results in a cluster bound to the surface with thermal energy less than the diffusion barrier (~0.1 eV) then the cluster will have limited mobility around the impact point. This will result in cluster binding to a thermodynamically favored position on the surface, and prevent large-scale diffusion and agglomeration into larger clusters. The selective adsorption sites suggest that bonding occurs between the cluster and one or more surface atoms.

Another possibility for cluster binding is that the surface does not recover completely to the normal 1×1 reconstruction during the relaxation process and that the cluster is

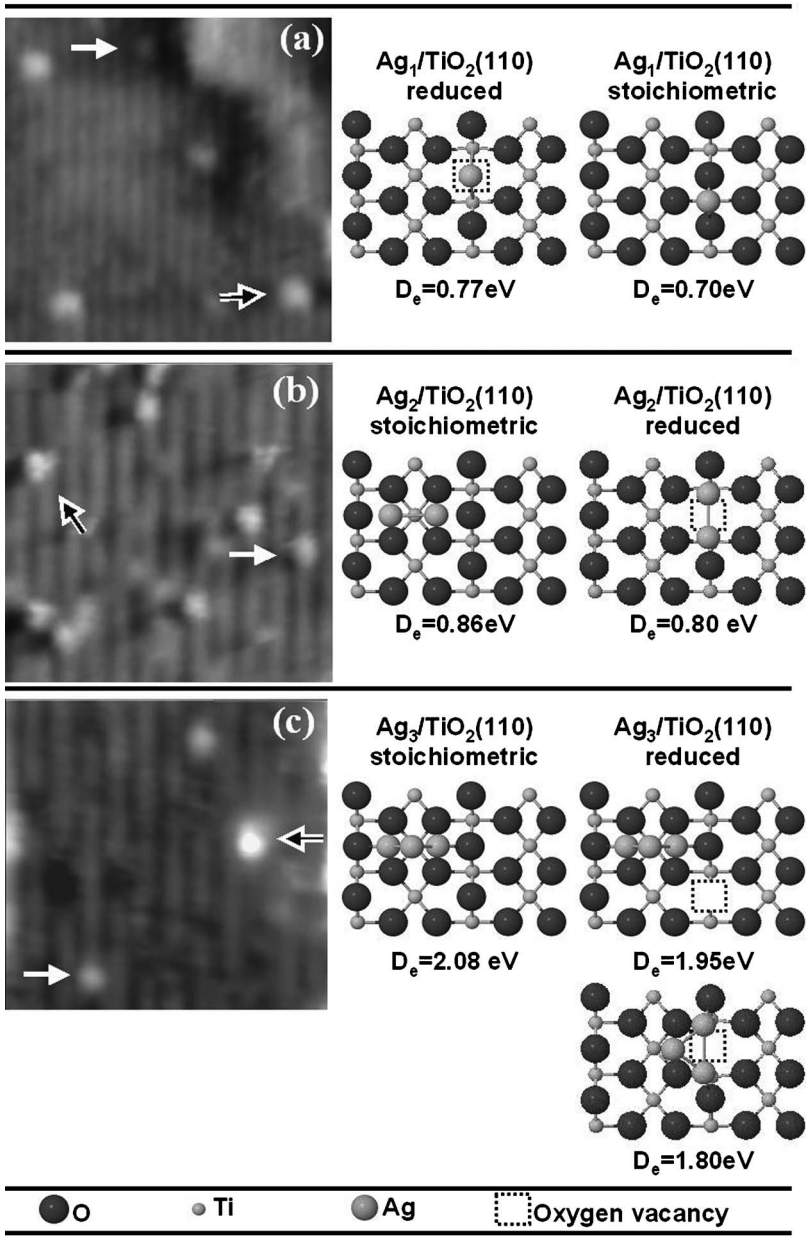

FIG. 3. High-resolution STM images: (a) (image size is 12×12 nm^2). Small clusters appear predominantly on bridging oxygen rows upon deposition of Ag_1 as indicated by the black arrow. The feature indicated with the white arrow is positioned above a 5*c*-Ti row. In images (b) and (c) (8 nm^2) small clusters mainly appear on 5*c*-Ti rows upon the deposition of Ag_2 and Ag_3 as indicated by the white arrows. The black arrows show clusters centered over bridging oxygen rows. The ball-and-stick models depict the lowest-energy structure corresponding to the adsorption of Ag_1 through Ag_3 on rutile $TiO_2(110)$ obtained from DFT calculations. The lowest-energy structure in which Ag_3 binds to a bridging oxygen vacancy is indicated also. D_e is the desorption energy of the cluster from the surface (see text for definition).

bound at a site of an impact-induced defect such as a displaced or missing surface atom. Adsorption sites determined from this model should be quite different than the thermodynamically favored sites on a pristine surface. As we discuss later in the text, this represents only a minor fraction of clusters on the surface.

When we increase the coverage of hard-landed silver clusters beyond ~5%, the cluster size increases at the cost of cluster density (not shown). This phenomenon can be explained by the above mechanism where local heating around the impact zone results in the aggregation of pre-existing small clusters with nearby later-arriving clusters. Detailed experimental demonstration of this local heating mechanism will be published elsewhere.

We performed DFT calculations to determine the adsorption geometries of Ag_1 through Ag_3 on the rutile $TiO_2(110)-(1\times1)$ surface. We looked at the adsorption on stoichiometric and reduced surfaces because Ag clusters land

TABLE I. Statistical results obtained from several STM images.

	Bright feature on bridging O rows		Bright feature on 5*c*-Ti rows	
Cluster size	Appearance frequency (%)	Height (Å)	Appearance frequency (%)	Height (Å)
Ag_1	65	1.75±0.50	35	1.12±0.17
Ag_2	11	1.74±0.44	89	1.36±0.14
Ag_3	4	1.79±0.23	96	1.03±0.13

either on a stoichiometric patch of the surface or near oxygen vacancies during the deposition and they possess low mobility according to the data in Figs. 2 and 3. Therefore, we expect the clusters to sit at the most stable position near the impact when equilibrium has been reached, i.e., when all the impact energies have been dissipated. For each cluster, we indicate only the lowest-energy structure corresponding to the adsorption on a stoichiometric and on reduced surfaces [a more detailed density-functional investigation of the binding of small Ag clusters on a stoichiometric and a reduced rutile $TiO_2(110)-(1\times1)$ surfaces will be published elsewhere].[31] The inclusion of all the significant isomers (e.g., looking at all the structures located in a window of 0.3 eV to take into account the limited accuracy of DFT) does not change the assignment of the bright spots observed in the STM images (Figs. 1–3).

The lowest-energy structures corresponding to the adsorption of Ag_1 on a stoichiometric and reduced surfaces are both centered on bridging oxygen rows. As shown in Fig. 3(a), DFT calculations reveal that Ag_1 prefers to bind at either an oxygen vacancy on a reduced surface with a desorption energy of 0.77 eV, or with two adjacent bridging oxygen atoms (in the same bridging oxygen row) on the stoichiometric surface with a desorption energy of 0.70 eV. Therefore, we assign the bright protrusions centered on bridging oxygen rows [Fig. 3(a)] to Ag atoms adsorbed at these two sites.

The question arises why 35% of the deposited Ag monomers are centered on 5*c*-Ti rows. DFT calculations indicate that the lowest-energy structures for these systems are 0.16 and 0.33 eV higher in energy than the bridging oxygen row sites for stoichiometric and reduced surfaces, respectively. Calculations using a slab of six layers (two triple layers) indicate diffusion barriers on the stoichiometric surface in the order of 0.1 eV. Consequently, Ag atoms above 5*c*-Ti rows readily diffuse to more stable bridging oxygen atom sites [Fig. 3(a)] at room temperature. One possible explanation for the experimental observation is that these atoms are bound to an impact-induced defect or even an impact-induced substitution of an Ag atom for one of the Ti atoms in a 5*c*-Ti row. DFT calculations indicate that this is the most stable Ag-atom substitution site on the rutile TiO_2 surface. This is a plausible explanation for the experimental data, but requires further energy-dependent impact studies and modeling of the STM image to confirm this suggestion.

As shown in Figs. 3(b) and 3(c) DFT calculations reveal that Ag_2 and Ag_3 prefer to bind between two adjacent bridging oxygen rows resulting in the appearance of the cluster centered on a 5*c*-Ti row. This is in agreement with the statistical analysis of various STM images (Table I) which indicates that between 89% and 96% of the bright features, observed after hard-landing depositions of Ag_2 and Ag_3, are centered on 5*c*-Ti rows.

The observed adsorption probabilities (Table I) of Ag_2 or Ag_3 centered on bridging oxygen rows are much lower than that of 5*c*-Ti rows (11% vs 89% for Ag_2 and 4% vs 96% for Ag_3). The opposite is observed for Ag_1. Based on DFT calculations (Fig. 3), this can be attributed to the fact that Ag_2 and Ag_3 prefer to bind between two adjacent bridging oxygen rows on a stoichiometric area of the surface rather than to a bridging oxygen vacancy. From Fig. 3(b) we can see that Ag_2 binds more strongly to the stoichiometric surface by 0.06 eV. The corresponding difference for the trimer is 0.28 eV. These desorption energy differences correlated with the fact that a larger fraction of the Ag_2 features are centered on bridging oxygen rows than Ag_3. The fact that the lowest-energy sites dominate the experimental observations we suggest that Ag_2 and Ag_3 have limited mobility on the surface. The observation that some higher-energy sites are populated is also consistent with a limited diffusion, nonequilibrium situation. Finally, this result is consistent with the fact that small features, attributed to intact Ag_3, were observed during soft-landing deposition of the trimer.[23]

The observed different adsorption sites of Ag_2 compared to Ag_1 indicate that hard-landed clusters of Ag_2 do not dissociate into fragments of Ag_1 upon impact. The apparent adsorption sites of Ag_3 are similar to that of Ag_2, but the apparent height is different (Table I). This implies that the Ag_3-substrate complex is different from that of Ag_2. In addition, there are practically no clusters centered on bridging oxygen rows, which we have shown to be the characteristic of Ag_1. Furthermore, intact, adsorbed Ag_3 clusters have also been observed on 5*c*-Ti rows in soft-landing experiments,[23] similar to the features observed here. These observations suggest that the hard-landed Ag_3 clusters do not dissociate into fragments of Ag_2 and/or Ag_1. These results are somewhat surprising. There is clearly sufficient energy to dissociate both Ag_2 and Ag_3 under our hard-landing conditions. If they do dissociate the silver products must remain close at hand and recombine as the damaged surface anneals itself. This is supported by DFT calculations, which indicate that the fragmentation of supported Ag_2 and Ag_3 is endothermic by more than 1 eV on the stoichiometric and reduced surfaces. An apparent lack of fragmentation has also been observed in the high-energy collision of Ag_2 with a solid substrate covered with a noble-gas film. The authors of that work assume dissociation followed by recombination occurs.[32] Cluster recrystallization from transient deformative states has also been found in MD simulations of different energetic cluster impacts on solid surfaces.[33,34]

VI. SUMMARY

We present a pinning mechanism of size-selected silver clusters hard landed on the $TiO_2(110)-(1\times1)$ surface at room temperature, which is observed with STM and supported by DFT calculations. In the case of the hard-landing experiments, sintering rarely occurs at low coverages ($<5\%$) and small clusterlike features appear on the surface without any observable surface damage. Statistically, Ag_1 prefers to bind on bridging oxygen rows while Ag_2 and Ag_3 prefer binding on 5*c*-Ti rows. After annealing at 600 K the smaller hard-landed clusters sinter to become larger clusters of about 40 atoms in size. No visible surface damage is apparent before or after annealing. Our observations suggest a self-recovery of the transiently damaged surface, as well as the segregation of potentially implanted clusters to the surface during thermalization. Some substitution of Ag for Ti in

5*c*-Ti rows for Ag_1 impact may occur during reconstruction. The energetically most stable adsorption geometries of Ag_n predicted by DFT calculations are consistent with our STM images for Ag_1, Ag_2, and Ag_3. The ability to fabricate monodispersed clusters via pinning of size-selected clusters opens an opportunity to study the catalytic activity of mass-selected Ag clusters on the $TiO_2(110)$ surface.

ACKNOWLEDGMENT

This work was funded by a Defense University of Research in Nanotechnology (DURINT) grant from the Air Force Office of Scientific Research (AFOSR).

[1] S. Lee, C. Fan, T. Wu, and S. L. Anderson, J. Am. Chem. Soc. **126**, 5682 (2004).
[2] P. Claus and H. Hofmeister, J. Phys. Chem. B **103**, 2766 (1999).
[3] W. Grünert, A. Brückner, H. Hofmeister, and P. Claus, J. Phys. Chem. B **108**, 5709 (2004).
[4] A. L. de Oliveira, A. Wolf, and F. Schüth, Catal. Lett. **73**, 157 (2001).
[5] D. A. Chen, M. C. Bartelt, S. M. Seutter, and K. F. McCarty, Surf. Sci. **464**, L708 (2000).
[6] J. T. Lau, W. Wurth, H.-U. Ehrke, and A. Achleitner, Low Temp. Phys. **29**, 223 (2003).
[7] R. Schaub, H. Jödicke, F. Brunet, R. Monot, J. Buttet, and W. Harbich, Phys. Rev. Lett. **86**, 3590 (2001).
[8] K. Bromann, H. Brune, C. Félix, W. Harbich, R. Monot, J. Buttet, and K. Kern, Surf. Sci. **377–379**, 1051 (1997).
[9] K. Bromann, C. Félix, H. Brune, W. Harbich, R. Monot, J. Buttet, and K. Kern, Science **274**, 956 (1996).
[10] B. Kaiser, T. M. Bernhardt, and K. Rademann, Appl. Phys. A: Mater. Sci. Process. **66**, S711 (1998).
[11] H. Jödicke, R. Schaub, A. Bhowmick, R. Monot, J. Buttet, and W. Harbich, Rev. Sci. Instrum. **71**, 2818 (2000).
[12] C. Xirouchaki, Vacuum **73**, 123 (2004).
[13] P. Kemper, A. Kolmakov, X. Tong, L. Benz, S. K. Buratto, and M. T. Bowers (unpublished).
[14] J. P. Perdew, J. A. Chevary, S. H. Vosko, K. A. Jackson, M. R. Pederson, D. J. Singh, and C. Fiolhais, Phys. Rev. B **46**, 6671 (1992).
[15] J. P. Perdew, K. Burke, and Y. Wang, Phys. Rev. B **54**, 16533 (1996).
[16] G. Kresse and J. Hafner, Phys. Rev. B **47**, 558 (1993).
[17] G. Kresse and J. Hafner, Phys. Rev. B **49**, 14251 (1994).
[18] G. Kresse and J. Furthmüller, Comput. Mater. Sci. **6**, 15 (1996).
[19] G. Kresse and J. Furthmüller, Phys. Rev. B **54**, 11169 (1996).
[20] D. Vanderbilt, Phys. Rev. B **41**, 7892 (1990).
[21] G. Makov and M. C. Payne, Phys. Rev. B **51**, 4014 (1995).
[22] H. Jónsson, G. Mills, and K. W. Jacobsen, in *Classical and Quantum Dynamics in Condensed Phase Simulations: Proceedings of the International School of Physics*, edited by B. J. Berne, G. Cicotti, and D. F. Coker (World Scientific, Singapore, 1998), p. 385.
[23] L. Benz, X. Tong, P. Kemper, Y. Lilach, A. Kolmakov, H. Metiu, M. T. Bowers, and S. K. Buratto, J. Chem. Phys. **122**, 081102 (2005).
[24] U. Diebold, J. Lehman, T. Mahmoud, M. Kuhn, G. Leonardelli, W. Hebenstreit, M. Schmid, and P. Varga, Surf. Sci. **411**, 137 (1998).
[25] U. Diebold, Surf. Sci. Rep. **48**, 53 (2003).
[26] R. A. Bennett, P. Stone, N. J. Price, and M. Bowker, Phys. Rev. Lett. **82**, 3831 (1999).
[27] H. Haberland, M. Karrais, M. Mall, and Y. Thurner, J. Vac. Sci. Technol. A **10**, 3266 (1992).
[28] H. Haberland, Z. Insepov, M. Karrais, M. Mall, M. Moseler, and Y. Thurner, Nucl. Instrum. Methods Phys. Res. B **80–81**, 1320 (1993).
[29] G. Betz and W. Husinsky, Nucl. Instrum. Methods Phys. Res. B **122**, 311 (1997).
[30] Y. Yamaguchi and J. Gspann, Phys. Rev. B **66**, 155408 (2002).
[31] S. Chrétien and H. Metiu (to be published).
[32] S. Fedrigo, W. Harbich, and J. Buttet, Phys. Rev. B **58**, 7428 (1998).
[33] H. P. Cheng, J. Chem. Phys. **111**, 7583 (1999).
[34] H. Haberland, Z. Insepov, and M. Moseler, Phys. Rev. B **51**, 11061 (1995).